Ultracold collisions of oxygen molecules

Alexandr V. Avdeenkov and John L. Bohn
JILA and Department of Physics, University of Colorado, Boulder, Colorado 80309
(Received 23 May 2001; published 2 October 2001)

Collision cross sections and rate constants between two ground-state oxygen molecules are investigated theoretically at translational energies below ~ 1 K and in zero magnetic field. We present calculations for elastic and spin-changing inelastic collision rates for different isotopic combinations of oxygen atoms as a prelude to understanding their collisional stability in ultracold magnetic traps. A numerical analysis has been made in the framework of a rigid-rotor model that accounts fully for the singlet, triplet, and quintet potential-energy surfaces in this system. The results offer insights into the effectiveness of evaporative cooling and the properties of molecular Bose-Einstein condensates, as well as estimates of collisional lifetimes in magnetic traps. Specifically, $^{17}O_2$ looks like a good candidate for ultracold studies, while $^{16}O_2$ is unlikely to survive evaporative cooling. Since $^{17}O_2$ is representative of a wide class of molecules that are paramagnetic in their ground state we conclude that many molecules can be successfully magnetically trapped at ultralow temperatures.

DOI: 10.1103/PhysRevA.64.052703 PACS number(s): 34.20.Cf, 34.50.−s, 05.30.Fk

I. INTRODUCTION

A. Background

Following the enormous successes of lowering the temperature of atoms to the submilliKelvin regime, experimental attention is now turning to producing ultracold molecular samples. The ''first generation'' of cold molecule experiments has now demonstrated the efficient production of cold samples by a variety of techniques, including photoassociation of ultracold atoms [1], counter-rotating supersonic jets [2], Stark slowing [3], and buffer-gas cooling [4]. The latter two have yielded trapped samples that are cold in rotational, vibrational, and translational degrees of freedom, although translational temperatures are still in the 0.1–1 K range.

The next generation of experiments will seek colder, denser samples. One option for cooling molecules further is the optical cooling strategy described in Ref. [5]. Alternatively, we consider in this paper the evaporative cooling of paramagnetic molecules in a static magnetic trap, following the strategies that have been employed to produce ultracold atoms. The central issue to the success of this method is that the rate of elastic, rethermalizing collisions far exceeds the rate of lossy inelastic collisions that produce untrapped, strong-field-seeking states. In terms of scattering rate coefficients, this criterion is usually written $K_{\rm el} > 10^2 K_{\rm loss}$. A large ratio of $K_{\rm el}/K_{\rm loss}$ is also vital for the stability of the trapped gas once it is cold. A main objective of this paper is to demonstrate that molecules with nonzero spin in their lowest energy state will be quite stable at ultralow temperatures.

We may reasonably assert that the elastic rate constants for neutral molecules have roughly the same magnitudes as those for neutral atoms, $K_{\rm el} \sim 10^{-12} - 10^{-10}$ cm^3/sec at low energies, barring unfortunately placed zeros in their *s*-wave scattering cross sections. Indeed, our calculations yield elastic rates of this magnitude. The spin-state-changing rate constants are, however, completely unknown for molecules at ultralow temperatures. To rectify this situation the present paper presents pilot calculations for cold collisions of molecular oxygen. This work is a logical next step following Refs. [6,7], which considered the interaction of molecular oxygen with a helium buffer gas.

Spin-state-changing cold collisions of O_2 molecules are driven by at least three distinct physical processes, two of which are already familiar from ultracold atom physics: (i) spin-exchange collisions, which typically lead to unacceptably large loss rates for both atoms and molecules; (ii) spin-spin magnetic dipolar interactions, which are typically small in either case; and (iii) spin-rotation interactions, unique to molecules, wherein electronic spins are influenced by their coupling to rotational motion, which is in turn dependent on torques exerted by the anisotropic potential-energy surface (PES) between the molecules.

Spin-exchange collisions can be avoided in cold molecule collisions, as in cold atom collisions, by preparing the molecules in their ''stretched'' states, with mechanical rotation, electronic spin, and nuclear spin (if any) all aligned along a common laboratory-fixed axis. We will therefore confine ourselves to this circumstance. By far the leading contribution to the rate constant for state-changing, lossy collisions ($K_{\rm loss}$) is then the spin-rotation coupling, as shown below in detailed calculations. Indeed, when an exothermic exit channel is available, this coupling can yield loss rates comparable in magnitude to spin-exchange rates, i.e., comparable to elastic collision rates. This is the case for the $^{16}O_2$ molecule. The spin-changing rate is, however, strongly suppressed when the only allowed exit channels are degenerate in energy with the incident channel and when the collision energy lies below a characteristic energy E_0. In the stretched state of $^{17}O_2$ this is indeed the case, since changing the molecular spin at low energy requires boosting the partial- wave angular momentum from $l=0$ to $l=2$. These collisions are therefore suppressed by the Wigner threshold law when $E < E_0$, where E_0 is the height of the $l=2$ centrifugal barrier. For $^{17}O_2$ the barrier is roughly $E_0 \sim 0.013$ K, not far below the temperature that buffer-gas cooling can take these molecules.

The potential for disaster in molecule cold collisions is far greater than in atom cold collisions. For example, hyperfine interactions are more complex, and include rotation-nuclear

spin couplings that can invert spins. These are, however, expected to have minimal impact on the stretched-state molecules. Also of potential significance are spin-vibration couplings, which we disregard in O_2 owing to the extremely large vibrational excitation energy of ground-state O_2 molecules compared to the energy available to excite them. The vibrational degrees of freedom remain to be fully explored at ultralow temperatures, but it is expected that vibrational quenching (also an exothermic process) can occur with appreciable rates [8]. Finally, polar molecules are susceptible to particularly strong long-range anisotropies. While this is not of direct relevance to molecular oxygen, it can be devastating to the electrostatic trapping of polar molecules [9], and potentially dangerous for magnetically trapped molecules when the electric and molecular dipole moments are coupled.

B. Oxygen molecules: General considerations

The importance of molecular oxygen as a potential candidate for cooling and trapping experiments has been emphasized elsewhere [6,10]. We will here consider O_2 molecules that have been cooled to temperatures below 1 K. We will, furthermore, assume that these molecules have relaxed to their electronic $^3\Sigma_g^-$ ground state and $v=0$ vibrational ground state. What remains are the rotational and spin degrees of freedom that influence evaporative cooling. In a typical magnetostatic trap the molecules can be confined provided that they are in a weak-field-seeking state, i.e., a state whose energy rises with magnetic field.

The Zeeman diagram of O_2 is reproduced in Fig. 1. Nuclear exchange symmetry declares that homonuclear oxygen isotopomers can have only even or only odd values of the nuclear rotation quantum number N [12]. For $^{16}O_2$ (or $^{18}O_2$), which has identical spin-zero nuclei, only odd values of N are allowed. For the isotopomer $^{17}O_2$, where each nucleus has spin $I_N=5/2$, the allowed N levels depend on the total nuclear spin $\vec{I}=\vec{I}_{NA}+\vec{I}_{NB}$. The molecules must have even values of N for odd values of I, and vice versa. Thus the lowest energy weak-field seeking states are $|N,JM_J\rangle = |1,22\rangle$ and $|1,21\rangle$ for $^{16}O_2$ or $^{18}O_2$, and $|N,JM_J\rangle=|0,11\rangle$ for $^{17}O_2$. These states are indicated by heavy lines in the figure.

Figure 1 illustrates the essential difference between the even-N and odd-N manifolds in O_2, from the standpoint of inelastic collisions. Namely, the trapped states with $J=2$ in the $N=1$ manifold can decay exothermically to the untrapped $J=0$ states. By contrast, the $N=0$ trapped state at low energy and low magnetic field can only change its spin projection M_J to other states that are nearly degenerate in energy. This difference proves crucial in strongly suppressing spin-rotation collisions in $^{17}O_2$ relative to $^{16}O_2$. This has already been discussed for cold collisions of O_2 with helium atoms [6,7]; the situation is similar when the molecules collide with each other. As in Refs. [6,7], we carry out calculations in zero magnetic field.

In this paper we ignore the role of nuclear spin, hence of hyperfine structure, in the $^{17}O_2$ isotopomer. This is justified by considering the molecules to be in their stretched states of $N=0$, with $M_J=J=1$ and $M_I=I=5$. The nuclear spin degrees of freedom are then frozen out. In principle the weak nuclear spin-rotation coupling would influence the nuclear spins, resulting in $F=6\rightarrow F=5,4$ transitions, but these couplings are an order-of-magnitude smaller than the spin-rotation couplings we are already considering. Moreover, measurements of the $^{17}O_2$ microwave spectrum [11] reveal that its hyperfine structure is inverted in its $N=0$ state, requiring that 3.7 mK of kinetic energy be supplied to change F. Thus at ultralow temperatures hyperfine-state-changing collisions are rigorously forbidden.

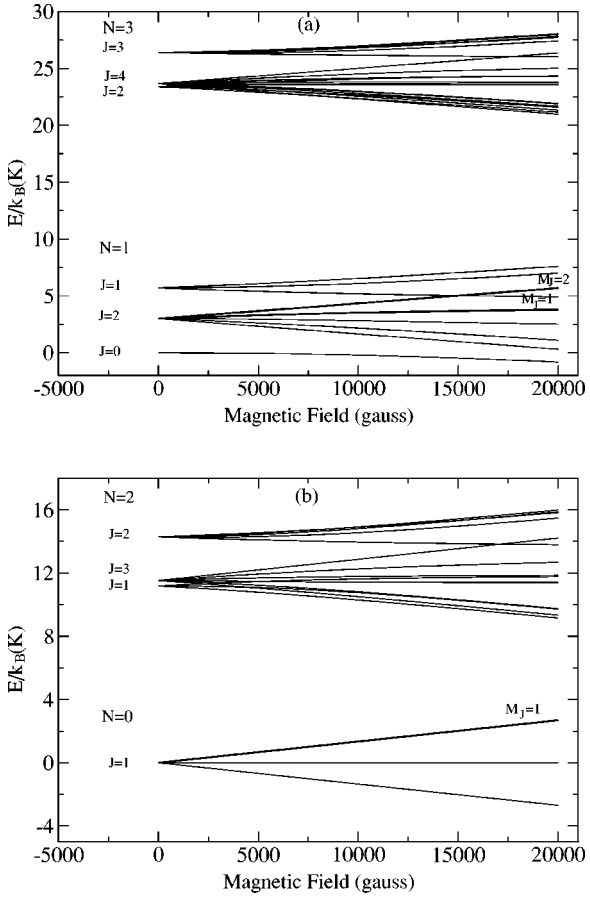

FIG. 1. The lowest-energy Zeeman levels of O_2 for odd-N (a) and even-N (b) rotational manifolds. The weak-field-seeking states of interest here are labeled by their M_J quantum numbers.

II. MODEL

A. Hamiltonian

Our investigation of molecular collisions follows the model of diatom-diatom scattering originally due to [13,14], but modified to incorporate the electronic spin of oxygen molecules. The $O_2(^3\Sigma_g^-)-O_2(^3\Sigma_g^-)$ dimer has a spin-dependent intermolecular potential, namely three potential surfaces exist corresponding to singlet ($S=0$), triplet ($S=1$), and quintet ($S=2$) states of total electronic spin S [15]. The complete Hamiltonian for the collision process can be written

$$H=T_A+T_B+V_s+V_{lr}+V_{dd}+H_{rfs}, \qquad (1)$$

where T_i is the translational kinetic energy of molecule i, V_s is the short-range exchange interaction, V_{lr} is the long-range potential consisting of dispersion and electric quadrupole-quadrupole interactions, V_{dd} is the electronic spin-spin dipolar interaction, and H_{rfs} is the Hamiltonian for the rotational fine structure of the two separate oxygen molecules. The hyperfine interaction will be disregarded for now, as was discussed above. The short-range potential can be written as a mean interaction plus exchange corrections, following Ref. [16]:

$$V_s(\mathbf{R},\omega_A,\omega_B,\mathbf{S_A},S_B)=V_{av}(\mathbf{R},\omega_A,\omega_B) - 2V_{ex}(\mathbf{R},\omega_A,\omega_B)\mathbf{S_A}\cdot S_B, \quad (2)$$

where $\omega=(\theta,\phi)$ are the polar angles of molecules A and B, respectively, $\mathbf{R}(R,\Theta)$ describes the radius vector between the center of mass of the molecules in the laboratory fixed coordinate frame and

$$V_{av}(\mathbf{R},\omega_A,\omega_B)=\sum_{L_A,L_B,L} f_{L_A,L_B,L}(R) \times(-1)^{L_B-L_A}\sqrt{(2L_A+1)(2L_B+1)} \times\mathbf{K^L}(\omega_A,\omega_B)\cdot\mathbf{C^L}(\Theta). \quad (3)$$

Here $K^L_M(\omega_A,\omega_B)=[C^{L_A}_{M_A}(\omega_A)\otimes C^{L_B}_{M_B}(\omega_B)]^L_M$ and C^L_M are reduced spherical harmonics. It should be said that the expansion (3) is identical to that in [16] but written in terms of reduced spherical harmonics. The spin-dependent Heisenberg exchange term V_{ex} is expanded similarly, but with a different expansion coefficient $g_{L_A,L_B,L}(R)$. The expressions for expansion coefficients $f_{L_A,L_B,L}(R)$ and $g_{L_A,L_B,L}(R)$ were obtained in the work of [15], and the quadrupole-quadrupole interaction has a similar form. The C_6 dispersion coefficients were calculated in [17] in the body-fixed frame. To unify our treatment we recast the anisotropic C_6 coefficients in terms of the same angular basis as the exchange potential

$$V_{disp}(\mathbf{R},\omega_A,\omega_B)=-\sum_{L_A,L_B,L}\frac{p_{L_A,L_B,L}}{R^6}(-1)^{L_B-L_A} \times\sqrt{(2L_A+1)(2L_B+1)} \times\mathbf{K^L}(\omega_A,\omega_B)\cdot\mathbf{C^L}(\Theta), \quad (4)$$

where

$$p_{L_A,L_B,L}=\sqrt{\frac{2L+1}{(2L_A+1)(2L_B+1)}} \times\sum_{M_A,M_B} d_{L_A,M_A,L_B,M_B}\begin{pmatrix} L_A & L_B & L \\ M_A & M_B & 0\end{pmatrix}. \quad (5)$$

The connection between our coefficients d_{L_A,L_B,M_A,M_B} and coefficients from [17] is in the Appendix. Figure 2 shows a slice through the potential-energy surface for the singlet states of the $[O_2(^3\Sigma_g^-)]_2$ dimer for the ''H'' geometry of the two molecules, which passes through the global minimum of the PES. Also shown are contributions to this potential from various components with different (L,L_A,L_B). We can see that this potential has a very strong anisotropy. Notice that the isotropic contribution, with $L_A=L_B=L=0$ accounts for less than half of the total well depth.

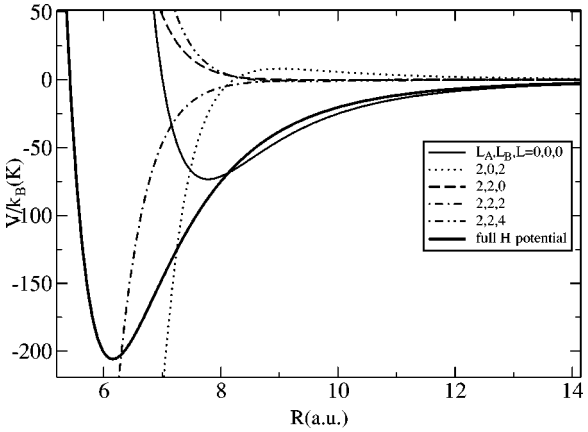

FIG. 2. The $O_2(^3\Sigma_g^-)$-$O_2(^3\Sigma_g^-)$ singlet potential for H geometry and the contributions from different sets (L_A,L_B,L).

As in the case of ultracold atoms, details of ultracold molecular collisions depend extremely sensitively on details of PES. Thus eventually the PES must be fine tuned using key experimental data to provide complete quantitative results [18,19]. Nevertheless, the order of magnitude of the rate constants, and their general trends, already emerge clearly in the present model.

The intermolecular spin-spin (magnetic dipole) interaction has the form [16]

$$V_{dd}(\mathbf{R},\mathbf{S_A},S_B)=-\frac{\sqrt{6}g_e^2\mu_B^2}{R^3}\mathbf{C^2}(\Theta)\cdot[\mathbf{S_A}\otimes S_B]^\mathbf{2}, \quad (6)$$

where $\mathbf{R}\equiv(R,\Theta)$, $g_e=2.0023$, and μ_B is the Bohr magneton. For alkali-metal atoms this is known to be a fairly weak contribution to spin-changing collisions, a conclusion that we find holds for molecules as well. Finally, in our model we take into account the molecular fine structure, which arises from the molecular rotation and spin-rotation coupling and is diagonal in our total-spin basis at large R. For $^{16}O_2$ we use the fine-structure constants determined in [20], and for $^{17}O_2$ we employ those determined in [21].

We express the Hamiltonian in a basis of total angular momentum,

$$\mathcal{J}=\mathbf{J}+\mathbf{l},$$
$$\mathbf{J}=\mathbf{J_1}+\mathbf{J_2},$$
$$\mathbf{J_i}=\mathbf{S_i}+\mathbf{N_i}, \quad (7)$$

in the terms of each molecule's mechanical rotation ($\mathbf{N_i}$), its electronic spin ($\mathbf{S_i}$), its total spin ($\mathbf{J_i}$), the combined spin for two molecules together ($\mathbf{J}$), and the partial wave represent-

ing the rotation of the molecule about the center of mass (**l**). In zero magnetic field both $\mathcal{J}$ and its laboratory-fixed projection $\mathcal{M}$ are rigorously conserved.

In this basis we can present our wave function as

$$\Psi_{\mathcal{J},\mathcal{M}}(R,\Theta,\omega_A,\omega_B,\sigma_A,\sigma_B) = \frac{1}{R}\sum_{l,\mathcal{J},J_1,J_2,N_1,N_2,S_1,S_2} \psi_{l,\mathcal{J},J_1,J_2,N_1,N_2,S_1,S_2} \times(R) I_{\mathcal{J},\mathcal{M};l,J,J_1,J_2,N_1,N_2,S_1,S_2}(\Theta,\omega_A,\omega_B,\sigma_A,\sigma_B), \tag{8}$$

where $\sigma_{A,B}$ represent the electronic spin coordinates for molecule A,B. The coupled angular momentum basis functions are defined by suitable tensor products

$$I_{\mathcal{J},\mathcal{M};l,J,J_1,J_2,N_1,N_2,S_1,S_2}(\Theta,\omega_A,\omega_B,\sigma_A,\sigma_B) = [P^J_{M_J}(\omega_A,\omega_B,\sigma_A,\sigma_B)\otimes Y^l_{m_l}(\Theta)]^{\mathcal{J}}_{\mathcal{M}}, \tag{9}$$

$$P^J_{M_J}(\omega_A,\omega_B,\sigma_A,\sigma_B) = [T^{J_1}_{M_{J_1}}(\omega_A,\sigma_A)\otimes T^{J_2}_{M_{J_2}}(\omega_B,\sigma_B)]^J_{M_J}, \tag{10}$$

$$T^{J_i}_{M_{J_i}}(\omega,\sigma) = [Y^{N_i}_{M_{N_i}}(\omega)\otimes\chi^{S_i}_{M_{S_i}}(\sigma)]^{J_i}_{M_{J_i}}, \tag{11}$$

where Y is a spherical harmonic and χ is a spinor wave function.

Because target and projectile are identical bosons, we must take into account the symmetry of the wave function under exchange. To this end we construct symmetrized angular momentum functions from Eq. (9)

$$I^s_{l,J,J_1,J_2,N_1,N_2,S_1,S_2} = \frac{I_{l,J,J_1,J_2,N_1,N_2,S_1,S_2} + (-1)^{J+J_1+J_2+l} I_{l,J,J_2,J_1,N_2,N_1,S_2,S_1}}{\sqrt{2(1+\delta_{J_1J_2}\delta_{N_1N_2}\delta_{S_1S_2})}}. \tag{12}$$

We have omitted the conserved quantum numbers $\mathcal{J},M$ in this expression.

To calculate the reduced matrix elements in our basis we recouple the angular part of the potential in terms of tensor elements:

$$K^L_M(\omega_A,\omega_B)[\mathbf{S_A}\cdot S_B]^\gamma = \sum_{J_A,J_B}\sqrt{[J_A][J_B]}(-1)^{L-L_A-J_B}\begin{Bmatrix} L_A & L_B & \gamma \\ J_B & J_A & L\end{Bmatrix}[T^{J_A}_{M_{J_A}}\otimes T^{J_B}_{M_{J_B}}]^L_{M_L}, \tag{13}$$

in terms of the spherical tensors $T^{J_A}_{M_{J_A}}(\omega_A,\sigma_A) = [Y^{L_A}_{M_{L_A}}\otimes[\chi^{S_A}_{M_{S_A}}]^\gamma]^{J_A}_{M_{J_A}}$, with $\gamma=0$ for V_{av} and $\gamma=1$ for the exchange part of the interaction (2), and $[Q]=(2Q+1)$.

Using our expansion of the intermolecular potential (3) and (4), the wave function (8), and taking into account the Wigner-Eckart theorem,

$$\langle\mathcal{J}\mathcal{M}|V_s+V_{disp}+V_{dd}|\mathcal{J}'M'\rangle = \delta_{\mathcal{J}\mathcal{J}'}\delta_{\mathcal{M}\mathcal{M}'}\langle\mathcal{J}||V_s+V_{disp}+V_{dd}||\mathcal{J}'\rangle, \tag{14}$$

we can present the reduced matrix elements for the V_s+V_{lr} part as

$$\begin{aligned}
&\langle\{[J_1(N_1S_1)J_2(N_2S_2)]Jl\}\mathcal{J}||(\mathbf{K^L}\cdot C^L)[\mathbf{S_A}\cdot S_B]^\gamma||\{[J_1'(N_1'S_1')J_2'(N_2'S_2')]J'l'\}\mathcal{J}\rangle \\
&= (-1)^{\mathcal{J}+J'-L_A+N_1+N_2}([l'][J'][l][J][J_1'][J_2'][J_1][J_2][N_1'][N_2'][N_1][N_2])^{1/2}\begin{Bmatrix} l & l' & L \\ J' & J & \mathcal{J}\end{Bmatrix}\begin{pmatrix} l & L & l' \\ 0 & 0 & 0\end{pmatrix} \\
&\times\begin{pmatrix} N_1 & L_A & N_1' \\ 0 & 0 & 0\end{pmatrix}\begin{pmatrix} N_2 & L_B & N_2' \\ 0 & 0 & 0\end{pmatrix}\sum_{J_AJ_B}(-1)^{J_B}[J_A][J_B]\begin{Bmatrix} L_A & L_B & \gamma \\ J_B & J_A & L\end{Bmatrix}\begin{Bmatrix} J & J' & L \\ J_1 & J_1' & J_A \\ J_2 & J_2' & J_B\end{Bmatrix}\begin{Bmatrix} J_1 & J_1' & J_A \\ N_1 & N_1' & L_A \\ S_1 & S_1' & \gamma\end{Bmatrix} \\
&\times\begin{Bmatrix} J_2 & J_2' & J_B \\ N_2 & N_2' & L_B \\ S_2 & S_2' & \gamma\end{Bmatrix}[\sqrt{S_A(S_A+1)(2S_A+1)S_B(S_B+1)(2S_B+1)}]^\gamma\delta_{S_1S_1'}\delta_{S_2S_2'},
\end{aligned} \tag{15}$$

and for the V_{dd} part as

$$\langle\{[J_1(N_1S_1)J_2(N_2S_2)]Jl\}\mathcal{J}||(C^2\cdot[S_A\otimes S_B]^2)||\{[J_1'(N_1'S_1')J_2'(N_2'S_2')]J'l'\}\mathcal{J}\rangle$$
$$=(-1)^{\mathcal{J}+J'+N_1+N_2+J_1+J_2}([l'][J'][l][J][J_1'][J_2'][J_1][J_2][2])^{1/2}\begin{Bmatrix} l & l' & 2 \\ J' & J & \mathcal{J}\end{Bmatrix}\begin{pmatrix} l & 2 & l' \\ 0 & 0 & 0\end{pmatrix}\begin{Bmatrix} J_1 & J_1' & 1 \\ 1 & 1 & N_1\end{Bmatrix}$$
$$\times\begin{Bmatrix} J_2 & J_2' & 1 \\ 1 & 1 & N_2\end{Bmatrix}\begin{Bmatrix} J & J' & 2 \\ J_1 & J_2 & 1 \\ J_1' & J_2' & 1\end{Bmatrix}\sqrt{S_A(S_A+1)(2S_A+1)S_B(S_B+1)(2S_B+1)}\,\delta_{S_1S_1'}\delta_{S_2S_2'}\delta_{N_1N_1'}\delta_{N_2N_2'}. \quad (16)$$

The reduced matrix elements of our potential between the states defined by Eqs. (8) and using (12) are

$$\langle\eta J_1J_2||U^s||\eta' J_1'J_2'\rangle=\frac{\langle\eta J_1J_2||U||\eta' J_1'J_2'\rangle+(-1)^{J+J_1+J_2+l}\langle\eta J_2J_1||U||\eta' J_1'J_2'\rangle}{\sqrt{(1+\delta_{J_1J_2}\delta_{N_1N_2})(1+\delta_{J_1'J_2'}\delta_{N_1'N_2'})}}\,\frac{1+(-1)^{N_1+N_2+l+N_1'+N_2'+l'}}{2}, \quad (17)$$

where η stands for the rest of the quantum numbers from our wave function (8). The coupling matrix element therefore vanishes between channels with different parity $(-1)^{N_1+N_2+l}$.

Figure 3 shows a partial set of adiabatic potential curves for $^{16}O_2$ in the case of $\mathcal{J}=0$. To generate this figure we include rotational channels $N=1,3,5$ and even partial waves $l=0-6$, which already imply 100 channels in this case. The strong anisotropy in the PES is here manifested mainly in a set of strongly avoided crossings near $R=8$ a.u. For $R>8$ a.u. the PES strongly favors a collinear configuration of the pair of molecules, while for $R<8$ a.u. it strongly favors a parallel, ''H''-shaped configuration. This figure stresses the importance of higher-lying rotational states in determining the details of scattering even at ultracold energies. However, for $^{16}O_2$ we have chosen to compute cross sections just for the case $l=0-10$, $N=1$ because these calculations already reveal very large spin-changing rates. Higher-lying channels will influence the details, but are unlikely to suppress losses. The total number of channels, including all values of $\mathcal{J}$, is then 212. For $^{17}O_2$, by contrast, we have computed cross sections for $l=0-10$ and $N=0,2$, to verify that higher-lying rotational states do not upset the observed suppression of loss rates. In this case the total number of channels considered is therefore 836.

B. Evaluating cross sections

We solve the coupled-channel equations using a logarithmic-derivative propagator method [22] to determine scattering matrices. Since we assume zero magnetic field the total angular momentum $\mathcal{J}$ is a good quantum number and the results are independent of the laboratory projection $\mathcal{M}$ of total angular momentum.

For magnetic trapping the molecular quantum numbers of interest are naturally the magnetic quantum numbers. Therefore we need to know the state-to-state cross sections in the $|N_1N_2J_1J_2,M_{J_1}M_{J_2}\rangle$ basis. The scattering matrices are readily converted to this basis,

$$\langle N_1N_2J_1J_2M_{J_1}M_{J_2}lM_l|\mathcal{S}|N_1'N_2'J_1'J_2'M_{J_1}'M_{J_2}'l'M_l'\rangle$$
$$=\sum_{JJ'}\langle J_1M_{J_1}J_2M_{J_2}|JM_J\rangle$$
$$\times\langle J'M_J'|J_1'M_{J_1'}J_2'M_{J_2'}\rangle\sum_{\mathcal{J}}\langle JM_JlM_l|\mathcal{J}M_{\mathcal{J}}\rangle$$
$$\times\langle\mathcal{J}M_{\mathcal{J}}|J'M_J'l'M_l'\rangle$$
$$\times\langle\{[J_1(N_1S_1)J_2(N_2S_2)]Jl\}\mathcal{J}\mathcal{M}|\mathcal{S}(\mathcal{J})|$$
$$\times\{[J_1'(N_1'S_1')J_2'(N_2'S_2')]J'l'\}\mathcal{J}\mathcal{M}\rangle. \quad (18)$$

For notational simplicity we define the index $\alpha=(N_1N_2J_1J_2)$ in the following. Then the complete symmetrized wave function in the limit of large R is given in [13]

$$\frac{\exp(i\vec{k}_\alpha\cdot\vec{R})T^{J_1}_{M_{J_1}}(\omega_A,\sigma_A)T^{J_2}_{M_{J_2}}(\omega_B,\sigma_B)+\exp(-i\vec{k}_\alpha\cdot\vec{R})T^{J_1}_{M_{J_1}}(\omega_B,\sigma_B)T^{J_2}_{M_{J_2}}(\omega_A,\sigma_A)}{\sqrt{2}}$$
$$+\sum_{\alpha' M'_{J_1}M'_{J_2}}\frac{\exp(ik'_\alpha R)}{R}\,\frac{f_{J_1'M'_{J_1}J_2'M'_{J_2}}(\hat{R})+f_{J_2'M'_{J_2}J_1'M'_{J_1}}(-\hat{R})}{\sqrt{2}}T^{J_1'}_{M_{J_1'}}(\omega_A,\sigma_A)T^{J_2'}_{M'_{J_2}}(\omega_B,\sigma_B), \quad (19)$$

where $f_{J_1'M_{J_1'}J_2'M_{J_2'}}$ is the channel-dependent scattering amplitude.

Using the definition of our wave function (8) and transforming it into the $|J_1J_2M_{J_1}M_{J_2}\rangle$ basis we can get the asymptotic form of the wave function in terms of the S matrix [13]

$$\sum_{\mathcal{J},J,l,M_l}\langle J_1M_{J_1}J_2M_{J_2}|JM_J\rangle \times\langle JM_JlM_l|\mathcal{J}\mathcal{M}_{\mathcal{J}}\rangle\sqrt{1+\delta_{J_1J_2}\delta_{N_1N_2}\delta_{M_{J_1}M_{J_2}}} \times\frac{4\pi}{2i\sqrt{k_\alpha}R}i^lY^l_{M_l}(\hat{k}_\alpha)\sum_{l',M_l'}\frac{1}{\sqrt{k_\alpha'}} \times\sum_{J',J_1',J_2'}\delta_{J_1J_1'}\delta_{J_2J_2'}\delta_{JJ'}\delta_{ll'}\exp[-i(k_\alpha'\cdot R-l'\pi/2] -\exp(i(k_\alpha'\cdot R-l'\pi/2) \times\langle\{[J_1J_2]Jl\}\mathcal{J}\mathcal{M}|\mathcal{S}(\mathcal{J})|\{[J_1'J_2']J'l'\}\mathcal{J}\mathcal{M}\rangle) \times I^s_{\mathcal{J},\mathcal{M};l',J',J_1',J_2'}(\Theta,\omega_A,\omega_B,\sigma_A,\sigma_B). \quad (20)$$

By comparing Eq. (19) with Eq. (20), we obtain the expression for the scattering amplitude

$$f_{J_1'M'_{J_1}J_2'M'_{J_2}}(\hat{R})+f_{J_2'M'_{J_2}J_1'M'_{J_1}}(-\hat{R}) =\frac{4\pi}{2i\sqrt{k_\alpha k_\alpha'}}\sum_{\mathcal{M},l,l'}\sqrt{1+\delta_{J_1J_2}\delta_{N_1N_2}\delta_{M_{J_1}M_{J_2}}} \times\sqrt{1+\delta_{J_1'J_2'}\delta_{N_1'N_2'}\delta_{M'_{J_1}M'_{J_2}}}Y^l_{M_l}(\hat{k}_\alpha)i^{l-l'} \times\langle N_1N_2J_1M_{J_1}J_2M_{J_2}lM_l|\mathcal{S} -\mathcal{I}|N_1'N_2'J_1'M'_{J_1}J_2'M'_{J_2}l'M_l'\rangle Y^{l'}_{M_l'}(\hat{R}), \quad (21)$$

where in the symmetrized separate-molecule basis the scattering matrix is given by

$$\langle N_1N_2J_1J_2M_{J_1}M_{J_2}lM_l|\mathcal{S}|N_1'N_2'J_1'J_2'M'_{J_1}M'_{J_2}l'M_l'\rangle =\frac{\sqrt{1+\delta_{J_1J_2}\delta_{N_1N_2}}}{\sqrt{1+\delta_{J_1J_2}\delta_{N_1N_2}\delta_{M_{J_1}M_{J_2}}}}\sum_{JJ'}\langle J_1M_{J_1}J_2M_{J_2}|JM_J\rangle \times\langle J'M_J'|J_1'M'_{J_1}J_2'M'_{J_2}\rangle\frac{\sqrt{1+\delta_{J_1'J_2'}\delta_{N_1'N_2'}}}{\sqrt{1+\delta_{J_1'J_2'}\delta_{N_1'N_2'}\delta_{M'_{J_1}M'_{J_2}}}} \times\sum_{\mathcal{J}}\langle JM_JlM_l|\mathcal{J}\mathcal{M}_{\mathcal{J}}\rangle\langle\mathcal{J}\mathcal{M}_{\mathcal{J}}|J'M_J'l'M_l'\rangle \times\langle\{[J_1(N_1S_1)J_2(N_2S_2)]Jl\}\mathcal{J}\mathcal{M}|\mathcal{S}(\mathcal{J}) \times\{[J_1'(N_1'S_1')J_2'(N_2'S_2')]J'l'\}\mathcal{J}\mathcal{M}\rangle. \quad (22)$$

Symmetrization in the $|J_1J_2M_{J_1}M_{J_2}\rangle$ basis requires that $J_1\geqslant J_2$ and that $M_1\geqslant M_2$ when $J_1=J_2$.

To obtain the scattering cross section we must integrate over the angular coordinates of the scattered wave. But, for undistinguishable final spin states we restrict the integral over half space ($\int d\Theta=2\pi$) to avoid double counting [23].

The total state-to-state cross section of interest for spin-rotational excitation and relaxation phenomena can be obtained using Eq. (21) from the $\mathcal{S}$ matrix

$$\sigma_{(N_1N_2)J_1J_2M_{J_1}M_{J_2}\to(N_1'N_2')J_1'J_2'M'_{J_1}M'_{J_2}} =\frac{(1+\delta_{J_1J_2}\delta_{N_1N_2}\delta_{M_{J_1}M_{J_2}})\pi}{k^2_{N_1N_2J_1J_2}} \times\sum_{lM_ll'M_l'}|\langle(N_1N_2)J_1M_{J_1}J_2M_{J_2}lM_l|\mathcal{S} -\mathcal{I}|(N_1'N_2')J_1'M'_{J_1}J_2'M'_{J_2}l'M_l'\rangle|^2, \quad (23)$$

where

$$k_{N_1N_2J_1J_2}=[2\mu(E-E_{N_1J_1}-E_{N_2J_2})]^{1/2} \quad (24)$$

is the channel wave number and $E_{N_{1,2}J_{1,2}}$ are fine-structure energy levels. In this expression we assume an average over all incident directions, as in [6]. Finally, state-to-state rate coefficients are given by

$$K_{(N_1N_2)J_1J_2M_{J_1}M_{J_2}\to(N_1'N_2')J_1'J_2'M'_{J_1}M'_{J_2}} =v_{(N_1N_2)J_1J_2}\sigma_{(N_1N_2)J_1J_2M_{J_1}M_{J_2}\to(N_1'N_2')J_1'J_2'M'_{J_1}M'_{J_2}}, \quad (25)$$

where $v_{(N_1N_2)J_1J_2}$ is the relative velocity of the collision partners before the collision.

III. RESULTS

This paper considers the scattering problem for the homonuclear species $^{16}O_2$ and $^{17}O_2$. References [6,7] speculated that buffer-gas cooling of O_2 by helium should be possible, thus lowering the molecules to typical temperatures $\approx$0.3 K. To further cool the gas by evaporative cooling requires favorabale collision rates for collision energies $E\lesssim 1$ K. We will limit our detailed calculations to this case. We will see that the cooling of $^{17}O_2$ could be quite efficient, while it is probably impossible for $^{16}O_2$.

A. $^{17}O_2$ elastic scattering

Since $^{17}O_2$ is the most promising candidate for evaporative cooling, we devote our attention to this isotopomer. We focus on the $|N_1N_2J_1J_2,M_{J_1}M_{J_2}\rangle=|0011,11\rangle$ state which is the lowest-lying trappable state for the even N-manifold (Fig. 1).

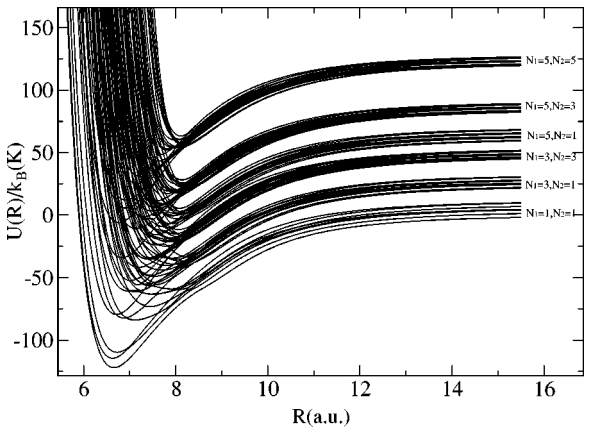

FIG. 3. A sample set of the adiabatic curves for $^{16}O_2$, in this case for total angular momentum $\mathcal{J}=0$. In computing these curves only the values $N=1,3,5$ and $l=0,2,4,6$ are included.

For identical bosons only even l-partial waves contribute to the cross sections for the $|0011,11\rangle$ state. A first important point of our calculations is to determine the number of partial waves that contribute to the cross section in the energy region up to 1 K and how many molecular rotational levels should be taken into account. In principle many partial waves are coupled together by the very anisotropic potential, but higher partial waves are suppressed at a low energy. Figure 4 illustrates the elastic cross sections for different values of the highest partial wave included. This figure shows that it is enough to include just $l=0-4$ partial waves for the qualitative description of the cross section in the region up to ≈ 0.2 K, and that the partial waves $l=0-10$ are sufficient in the region up to ≈ 1 K. For all our calculations for $^{17}O_2$ we considered just the two lowest rotational levels $N=0,2$. Including only the $N=0$ rotational level allows the molecules to explore only the isotropic part of their PES. Thus $N=2$ states must be included at least. The influence of higher rotational levels are found to be small in test calculations, although they impact details of the resonance structure. The calculations thus include 836 channels.

Particularly striking in Fig. 4 is the strong difference in the cross sections when $l_{max}=2$ as opposed to l_{max}

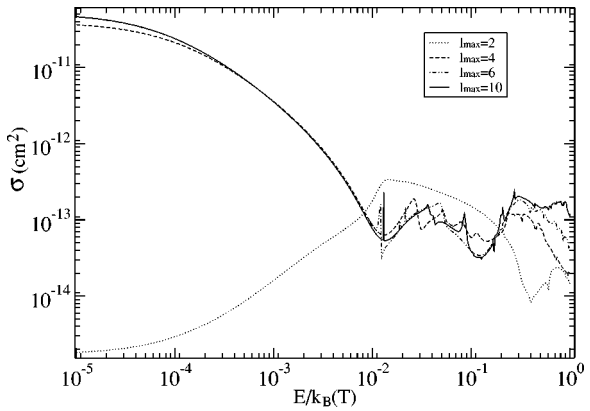

FIG. 4. Elastic scattering cross sections versus energy for different l_{max} for $^{17}O_2$. For example, $l_{max}=6$ means that $l=0,2,4,6$ partial waves were taken into account. See text for details.

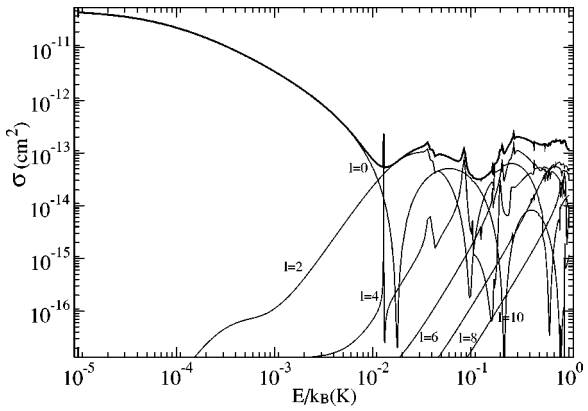

FIG. 5. Elastic partial-wave cross sections for $^{17}O_2$ molecules in their magnetically trapped $|0011,11\rangle$ state. Odd-l contributions do not exist for this state because of the identical-boson exchange symmetry.

$=4,6,8,10$. This is caused by the strong anisotropy of the potential [15] and mathematically this means that for the case $l_{max}=2$ we take into account only a small number of expansion functions (L,L_A,L_B) in Eq. (3). Although these few functions represent ''most'' of the potential, even small changes in potential can change the behavior of the cross section dramatically near zero energy [19]. Figure 5 shows the elastic cross sections for $|0011,11\rangle$ collisions and the contribution from different partial waves. We can see that the partial waves $l=8$ and $l=10$ contribute significantly only above ≈ 0.5 K.

Figure 5 also exhibits dozens of resonances for molecular-molecular collisions below 1 K, arising from the enormous number of internal molecular states [7]. Although we do not assign quantum numbers to the resonant states here, we expect them to be of two basic types, as discussed in [7]: (i) coupled-channel shape resonances; (ii) ''rotational Feshbach'' resonances that change the value of N of one or more molecules. This last type of resonance can be extremely long lived, owing to the difficulty of both molecules returning to their rotationless state in a collision. We will return to this subject in a future publication.

Figure 5 shows that the elastic cross section has a very large value near zero energy, corresponding to a scattering length $a=270$ a.u. in the present model. It is therefore possible that there may be an s-wave bound state in the region of negative energies near the threshold of the channel. In this case the cross section should have $\sim 1/(E+|\varepsilon|)$ dependence [24] on energy E and on the energy of the bound state ε.

We have included the dipole-dipole interaction in these calculations. However, the role of this interaction is very small in general, influencing the cross section at the 1% level and shifting resonance positions slightly. Likewise, this interaction is only a small perturbation to inelastic scattering.

B. $^{17}O_2$ prospects for evaporative cooling

For the $|N_1N_2J_1J_2,M_{J_1}M_{J_2}\rangle=|0011,11\rangle$ state of interest to trapping experiments, N_i and J_i are conserved at low energy, since the next energetically available state (with N

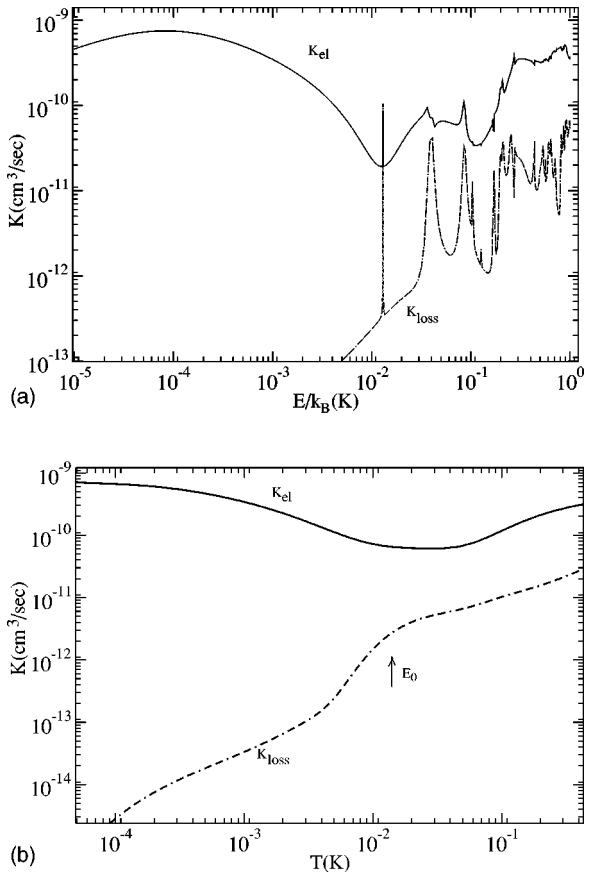

FIG. 6. (a) Rate constants versus energy for $^{17}O_2$-$^{17}O_2$ collisions with molecules initially in their $|0011,11\rangle$ state. (b) The thermally averaged elastic and loss rates from (a) as a function of temperature. Elastic collisions strongly dominate spin-changing loss collisions at low temperatures. E_0 denotes the energy, in Kelvin units, of the height of the $^{17}O_2$ d-wave centrifugal barrier.

$=2$) is 11.18 K higher in energy (Fig. 1). Thus the only possible final states are those that differ from the initial one in their projections M_{J_1} and M_{J_2}. To accomplish such a transition therefore requires that the angular momentum be carried away in the orbital angular momentum l. Furthermore, the collisions that originate in s-wave channels will be suppressed at energies below the centrifugal barrier of the d-wave exit channel. Using an effective C_6 coefficient, C_6^{eff} from [17] this energy for a partial wave l can be approximated as

$$E_0(l)=\frac{\hbar^2 l(l+1)}{2mr_b^2}-\frac{C_6^{eff}}{r_b^6}, \quad r_b^2=\sqrt{\frac{6C_6^{eff}m}{\hbar^2 l(l+1)}}. \quad (26)$$

For O_2, $C_6^{eff}=80.5$ a.u. and the d-wave threshold energy is 0.013 K.

The main aim of this paper, as previously discussed, is to compare the elastic and loss rate constants. Figure 6(a) shows these rates calculated according to Eq. (25). Away from resonances, in the energy range up to $E_0\approx 0.013$ K the loss rate constant is indeed strongly suppressed. A detailed examination of the final states contributing to this loss reveals general features which are the similar to those for He-$^{17}O_2$ scattering. Namely, elastic scattering, which does not change either M_{J_1} or M_{J_2}, is the most probable result of a collision. The next most likely processes are those for which the final M_J differs from the initial one by 1 or 2 and the rates for these processes are smaller than the elastic rate by 1–2 orders of magnitude. The processes for which the final M_J differs from the initial one by 3 or 4 have rates smaller than for elastic scattering by 2–4 orders of magnitude. For energies above ≈ 0.013 K inelastic processes become more probable, with rates only about 7–10 times smaller than elastic rates.

The thermally averaged elastic and loss rates are relevant to the experimental situation. If we assume the velocity distribution is Maxwellian characterized by a kinetic temperature T we can calculate the thermally averaged rate constant as

$$\overline{K}(T)=\left(\frac{8k_BT}{\pi m}\right)^{1/2}\frac{1}{(k_bT)^2}\int_0^\infty E\sigma(E)e^{-E/k_BT}dE. \quad (27)$$

To do this averaging we extrapolate the cross sections to energies greater than 1 K using their values at $E=1$ K.

Figure 6(b) shows these thermally averaged elastic and loss rates. For the cooling to be efficient the rate of elastic collisions K_{el} must exceed the rate of spin-changing, lossy collisions K_{loss} by at least two orders of magnitude [25]. For $^{17}O_2$, below $T\approx 0.01$ K this condition is fulfilled. However, there is a "relatively dangerous temperature range" above ≈ 0.01 K where $K_{el}/K_{loss}\approx 7-10$. By comparison, consider the equivalent ratio for He-O_2 scattering, as discussed in Ref. [7]. The fact that K_{el}/K_{loss} is not so large as for He-O_2 collisions originates from the stronger anisotropy and the deeper PES for the O_2-O_2 system. It remains to be seen if the loss rates are sufficiently low to evaporatively cool from buffer-gas temperatures, ≈ 0.3 K, down to $T<0.01$ K, where cooling should be quite efficient.

C. $^{16}O_2$

It is a different situation for $^{16}O_2$ molecules from the point of view of comparing elastic and inelastic cross sections. The general behavior of the elastic cross section for different channels is similar to that of $^{17}O_2$ and has the same order of magnitude except in the energy region near zero which is very sensitive to the details of the potential and the reduced mass. With the present PES the $^{16}O_2$ scattering length is 28 a.u.

Figure 7 shows the elastic and all the inelastic cross sections for the trapped state $|N_1N_2J_1J_2,M_{J_1}M_{J_2}\rangle=|1122,22\rangle$. The total number of inelastic channels is 25. When the final states are $|1120,20\rangle$, $|1100,00\rangle$, $|1110,10\rangle$, and so on, i.e., when at least one of the molecules changes to the $J=0$ state, the collision is superelastic. It is well known that for a superelastic channel there is "$\sigma\sim 1/v$" threshold law. Thus at a low energy there is a substantial loss of molecules from the $|1122,22\rangle$ state. The same result holds for the $|1122,11\rangle$ state which is also, of course, susceptible to spin exchange. Thus

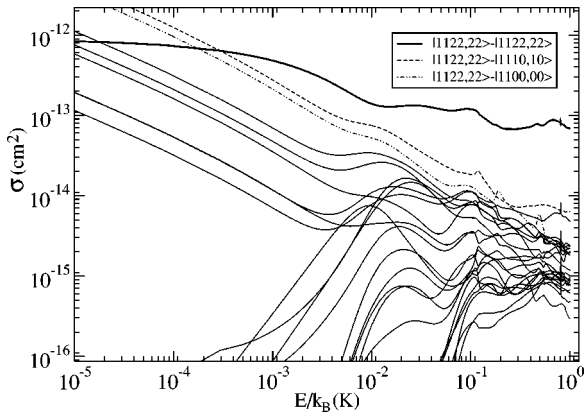

FIG. 7. Elastic scattering cross sections and all inelastic scattering cross sections for the initial $|1122,22\rangle$ state of $^{16}O_2$. Here channels with $l_{max}=10$, $N=1$ are included.

$^{16}O_2$ is clearly unstable against collisional losses in a magnetic trap, in sharp contrast to $^{17}O_2$. The cross sections for the stretched states of $^{16}O_2$ molecules that we are interested in have a smooth structure in the energy region up to 1 K, implying either a lack of resonances in this region or their large widths. From Fig. 7 we can see just one sharp Feshbach-type resonance near ≈ 0.8 K belonging to an $l=10$ bound state. Although there may be other weak resonances, it was not our aim to find all the resonances and identify their nature in this paper.

IV. CONCLUSION

In this paper we theoretically investigated ground-state diatom-diatom collisions in the energy range up to 1 K taking different isotopomers of oxygen molecules as a prototype. The main point of our investigation was to estimate the ratio of elastic and inelastic rate constants. The influence of the rotational degrees of freedom is crucial in determining this ratio. In the case of the odd N manifold, it is probably impossible to satisfy the criterion $K_{\rm el} > 10^2 K_{\rm loss}$ for stretched states in any energy region because of both the strong anisotropy of the PES and the existence of the superelastic channels. In the case of the even N manifold, namely $N=0$, this criterion can be fullfilled because for the stretched state $|0011,11\rangle$ there are no superelastic channels.

Even though the required ratio of $K_{\rm el}/K_{\rm loss}$ is not quite met at buffer-gas temperatures, it is worth remembering that the buffer-gas procedure typically produces a far larger sample of trapped molecules than do the laser-cooling experiments on which evaporative cooling is usually applied. Thus it is possible that a larger loss rate could be sustained without harming the overall yield of molecules at ultralow temperatures. Detailed rate-equation simulations of the cooling process are therefore required, an item to which we will turn our attention in the future.

Equally important, once the molecules have in fact been cooled to μK temperatures, our results imply that the lossy collision rates have diminished into insignificance, falling to levels well below 10^{-14} cm^3/sec. This in turn implies that ultracold spin-polarized $^{17}O_2$ gases, like their atomic counterparts, are experimentally stable and should allow the production of novel Bose-Einstein condensates.

Beyond the immediate results for our particular model of $^{17}O_2$, the present results have broad implications for many paramagnetic molecular species. Namely, the characteristic suppression of loss rates below the *d*-wave centrifugal barrier should be a generic feature for molecules where no superelastic fine-structure-changing processes exist. It is also important to assess in detail the influence of the anisotropy of the PES. For this purpose further investigations are necessary.

ACKNOWLEDGMENT

This work was supported by the National Science Foundation.

APPENDIX: THE DEFINITION OF THE COEFFICIENTS

Using the dispersion contribution part from [17] and expanding this part in the terms of spherical reduced harmonics (4) in the laboratory-fixed coordinate frame we defined the connection between our coefficients d_{L_A,M_A,L_B,M_B} and coefficients A,B,C from [17]

$$d_{0,0,0,0}=\frac{1}{3}(2A+8B+8C); d_{2,0,2,0}=2A-4B+2C,$$

$$d_{2,0,0,0}=d_{0,0,2,0}=\frac{1}{3}(2A+2B-4C),$$

$$d_{2,-1,2,1}=d_{2,1,2,-1}=\frac{1}{3}(4A-8B+4C),$$

$$d_{2,-2,2,2}=d_{2,2,2,-2}=\frac{1}{3}(2A-4B+2C).$$

[1] A. Fioretti *et al.*, Phys. Rev. Lett. **80**, 4402 (1998); T. Takekoshi, B. M. Patterson, and R. J. Knize, *ibid.* **81**, 5105 (1998); Phys. Rev. A **59**, R5 (1999); A. N. Nikolov *et al.*, Phys. Rev. Lett. **82**, 703 (1999); R. Wynar *et al.*, Science **287**, 1016 (2000).

[2] M. Gupta and D. Herschbach, J. Phys. Chem. A **103**, 10 670 (1999).

[3] H. L. Bethlem, G. Berden, and G. Meijer, Phys. Rev. Lett. **83**, 1558 (1999); H. L. Bethlem *et al.*, Nature (London) **406**, 491 (2000).

[4] J. M. Doyle, B. Friedrich, J. Kim, and D. Patterson, Phys. Rev. A **52**, R2515 (1995); J. D. Weinstein, *et al.*, J. Chem. Phys. **109**, 2656 (1998); D. Egorov, J. D. Weinstein, D. Patterson, B. Friedrich, and J. M. Doyle, Phys. Rev. A **63**, 030501(R) (2001).

[5] Vladan Vuletic and Steven Chu, Phys. Rev. Lett. **84**, 3787

(2000).
[6] J. L. Bohn, Phys. Rev. A **61**, 040702 (2000).
[7] J. L. Bohn, Phys. Rev. A **62**, 032701 (2000).
[8] N. Balakrishnan, R. C. Forrey, and A. Dalgarno, Phys. Rev. Lett. **80**, 3224 (1998); R. C. Forrey, V. Kharchenko, N. Balakrishnan, and A. Dalgarno, Phys. Rev. A **59**, 2146 (1999); R. C. Forrey *et al.*, Phys. Rev. Lett. **82**, 2657 (1999).
[9] J. L. Bohn, Phys. Rev. A **63**, 052714 (2001).
[10] B. Friedrich, R. deCarvalho, J. Kim, D. Patterson, J. D. Weinstein, and J. M. Doyle, J. Chem. Soc., Faraday Trans. **94**, 1783 (1998).
[11] G. Cazzoli, C. Degli Esposti, and B. M. Landsberg, Nuovo Cimento D **3**, 341 (1984).
[12] M. Mizushima, *The Theory of Rotating Diatomic Molecules* (Wiley, New York, 1975).
[13] K. Takayanagi, Adv. At. Mol. Phys. **1**, 149 (1965).
[14] T. G. Heil, S. Green, and D. J. Kouri, J. Chem. Phys. **68**, 2562 (1978).
[15] Paul E. S. Wormer and Ad van der Avoird, J. Chem. Phys. **81**, 1929 (1984).
[16] A. van der Avoird and G. Brocks, J. Chem. Phys. **87**, 5346 (1987).
[17] B. Bussery and P. E. S. Wormer, J. Chem. Phys. **99**, 1230 (1993).
[18] Markus Meuwly and Jeremy M. Hutson, J. Chem. Phys. **110**, 8338 (1999).
[19] A. V. Avdeenkov and J. L. Bohn (unpublished).
[20] M. Tinkham and W. P. Strandberg, Phys. Rev. **97**, 937 (1955); **97**, 951 (1955).
[21] G. Cazzoli and C. Degli Esposti, Chem. Phys. Lett. **113**, 501 (1985).
[22] B. J. Johnson, J. Comput. Phys. **13**, 445 (1973).
[23] J. P. Burke, Jr., Ph.D. thesis, University of Colorado, 1999.
[24] L. D. Landau and E. M. Lifshitz, *Quantum Mechanics: Non-Relativistic Theory*, 4th ed. (Nauka, Moscow, 1989).
[25] C. R. Monroe, E. A. Cornell, S. A. Sackett, C. J. Myatt, and C. E. Wiemann, Phys. Rev. Lett. **70**, 414 (1993).